http://dx.doi.org/10.5012/bkcs.2014.35.8.2555

Improvement of Signal Stability by a Cyclone-type Particle Separator for Ceramic Analysis using Laser Ablation ICP-MS

Jin Sook Lee and H. B. Lim*

*Department of Chemistry, Dankook University, Jukjeon 448-701, Korea. *E-mail: plasma@dankook.ac.kr*
Received March 13, 2014, Accepted April 11, 2014

Key Words : Particle separator, Ceramic powders, Laser ablation, Signal stability

Laser ablation as a sample introduction in ICP-MS has the advantages of short analysis time and less labor owing to direct solid sampling. Especially chemical resistant materials like ceramics and special ores have been subjected to typical targets for laser ablation because it is difficult to decompose them by acids for homogeneous aqueous sampling.[1,2] The ablated particles, however, are generally irregular in size, which causes the fluctuation of signals in ICP-MS measurement, resulting in low precision and large experimental error.[3,4] In the case of ingot or solid samples, it showed fairly stable signals and produced reasonable analytical results. Typically, most ceramic samples in the market are powder form which generates more particles than ingot samples. Such phenomena directly influence upon the signal intensity and stability of the measurement.[5] Among many trials to improve the analytical performance, particle separators or signal stabilizers have attracted interest for powder analysis by laser ablation.[6,7] Reportedly, a baffled-type, a coil-type or a cylindrical type particle separation device was used as a particle filter which functioned like a spray chamber for liquid sample introduction.[8] They filtered out large and heavy particulates or agglomerates by collision on baffle or gravity. Those techniques can reduce the fluctuation of ICP-MS signal and increase the signal stability.

In this study a cyclone-type particle separator was newly designed to introduce the ablated particles as shown in Figure 1. It was made of quartz with the dimension of 50 mm in diameter and 40 mm in height. Its shape and size was similar to the cyclone type spray chamber. It mostly filtered the heavy particles out by centrifugal force. And, those particles were also forced to bump against the separator wall and collected at the bottom chamber by gravity. The particles passed through the separator would be dissociated and ionized completely in ICP-MS. In order to study the analytical performance, the signal intensities and the relative standard deviations (RSD) were observed in this work as the ablation cell gas was changed to Ar or He. In addition, the size distribution of the generated particles was examined by scanning electron microscopy (SEM).

Four ceramic powder samples were pelletized and analyzed in this work. Each sample has different matrix and particle size. For example, AES12 (500 nm) and AL-41 (40-60 mm) of alumina were selected to investigate the effect of sample particle size because there were chemically similar to each other and highly pure. And, indium tin oxide (ITO, 50 nm) and magnesia (MgO, 1 mm) powders were also tested.

As shown in Figures 2 and 3, regardless of cell gas, the designed cyclone-type particle separator showed no signal change in both nano-sized ceramic powders, ITO and AES12, whereas it increased the signal intensities for the micro-sized

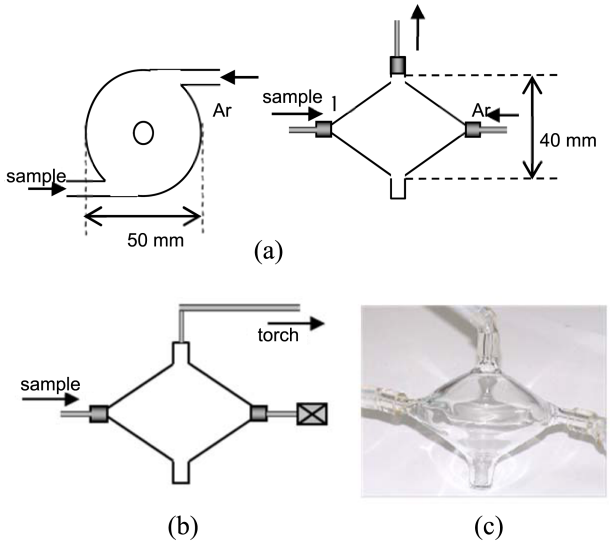

Figure 1. Designed cyclone-type particle separators: schematic diagram of He atmosphere (a) and Ar atmosphere (b) and a photograph (c).

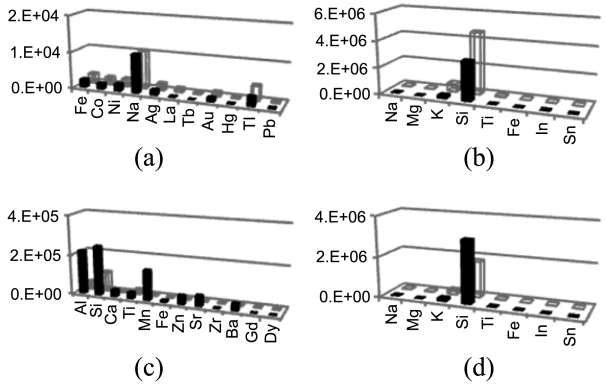

Figure 2. Effect of the designed particle separator on the signal intensities of ceramic powders in He atmosphere: (a) ITO, (b) AES12, (c) MgO, and (d) AL-41. Data with the separator was in black (front) and without it in open (back) bars.

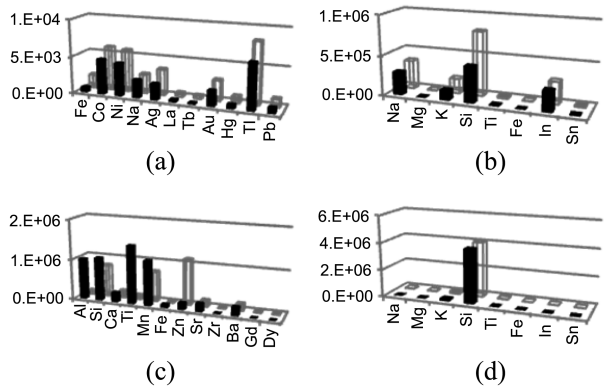

Figure 3. Effect of the designed particle separator on the signal intensities of ceramic powders in Ar atmosphere: (a) ITO, (b) AES12, (c) MgO, and (d) AL-41. Data with the separator was in black (front) and without it in open (back) bars.

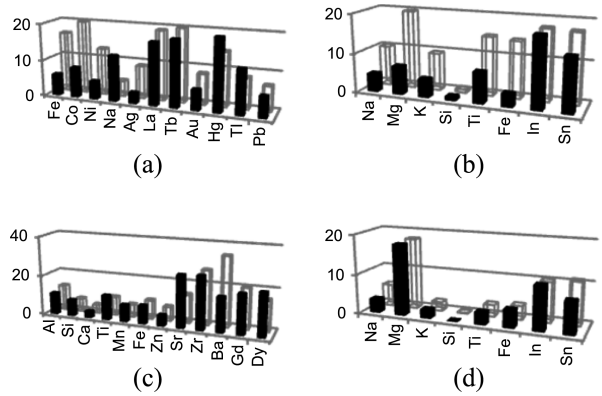

Figure 5. Relative standard deviations of signal intensity in Ar atmosphere when the particle separator was used (black bars) and not used (open bars): (a) ITO, (b) AES12, (c) MgO, and (d) AL-41.

particles, MgO and Al-41. This result indicated that the pellets made of nano-sized powders produced small particulates which were transported efficiently and ionized well in the plasma. Therefore, the nano-sized powder samples can be analyzed quantitatively by LA-ICP-MS no matter whether the particle separator was used or not.

On the contrary, the micron-sized MgO powders showed the increase of signal intensity in Ar atmosphere when the particle separator was used. AL-41 showed weak signal intensities for all the elements with no significant change. This result can also be explained by the difference in transport efficiency of the ablated particles. The heavy particles with high density produced low transport efficiency, which resulted in low signal intensities. Noticeably, the tap density of MgO powder was smaller than that of AL-41, as listed in Table 1. In addition, we observed white powders remained in the ablation chamber after ablating AL-41 whereas no residue powders were observed in the chamber after ablating MgO. The ablated AL-41 particles might be too heavy to be transported through particle separator.

Since one of the main purposes of this work was to improve the measurement stability, the relative standard deviations were measured. Figure 4 and Figure 5 illustrated the analytical results for the powder samples.

When the separator was used in He, both the micron-sized powder samples, MgO and AL-41, showed the significant decrease of RSD (Fig. 4(c) and (d)), because the large particles were removed by the centrifugal force. However, the nano-sized powder samples (Fig. 4(a) and (b)) showed no difference because the ablated particles were too small to be trapped in the particle separator, as expected.

On the contrary, in the case of Ar, the RSD for nano-sized powder samples (Fig. 5(a) and (b)) was reduced by the particle separator and the micron-sized power samples showed almost no change. Interestingly, this result was the opposite of the He environment. Reportedly, He produced more fine and homogeneous particles than Ar gas did,[9-13] because of their different physical properties. He gas has higher thermal conductivity, about 10 times lower density, and higher ionization potential than Ar gas. Whereas, the ablated particles, even small nanoparticles, were so easily condensed at the wall of the particle separator when Ar was used.[14] Therefore He gas produced smaller particles with homogeneous size distribution for the nano-sized powders, compared to Ar gas.

For the micron-sized powder, those gas effecs were diminished due to the large particle size of sample powder.

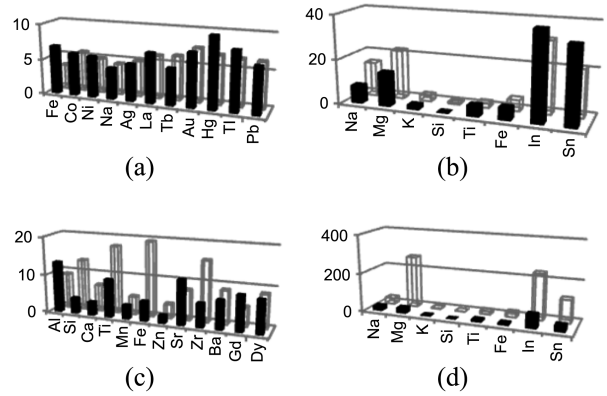

Figure 4. Relative standard deviations of signal intensity in He atmosphere when the particle separator was used (black bars) and not used (open bars): (a) ITO, (b) AES12, (c) MgO and (d) AL-41.

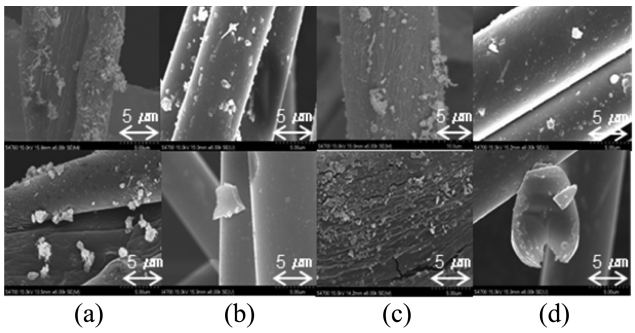

Figure 6. SEM images of the ablated particles in He gas flow with the particle separator (top) and without the separator (bottom): (a) ITO, (b) AES12, (c) MgO, and (d) AL-41.

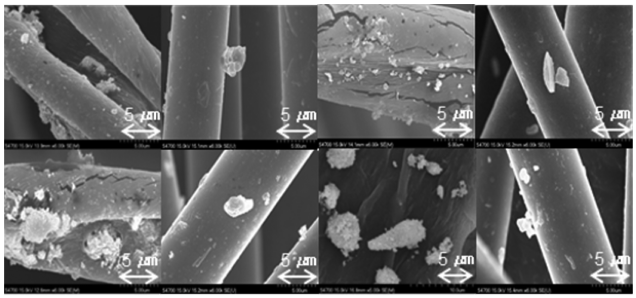

(a) (b) (c) (d)

Figure 7. SEM images of the ablated particles in Ar gas with the particle separator (top) and without the separator (bottom): (a) ITO, (b) AES12, (c) MgO, and (d) AL-41.

In order to clarify the correlation between the cell gas and the particle separator, SEM images of the ablated particles trapped at the outlet were taken as shown in Figures 6 and 7. From the images of Figure 6, no big clusters were observed in He atmosphere even when particle separator was not used. However, AL-41 produced large particles compared to the other samples, MgO, ITO and AES-12, when particle separator was not used. In addition, the size of trapped particles were reduced with the use of particles separator, which indicated that the particle separator eliminated the large particles efficiently in a He gas flow. Noticeably, the trapped particles were relatively small in size with homogeneous distribution.

Compared to them, the ablated particles of the nano-sized powders, as shown in Figure 7, were relatively large and agglomerated even though the particle separator was used.

This result agreed with the explanation discussed above, *i.e*., the small particles ablated from the nano-sized powders became aggregated and produced the large RSD in Ar gas. In the case of large and heavy powder sample, AL-4, no significant effect of the separator was observed (Fig. 7(d)).

Figure 7 SEM images of the ablated particles in Ar gas with the particle separator (top) and without the separator (bottom): (a) ITO, (b) AES12, (c) MgO, and (d) AL-41.

Interestingly the SEM image of the particles produced by MgO in Ar atmosphere showed big clusters when the separator was not used. Since the density of MgO was relatively low compared to AL-41, the sizes of ablated particles were relatively small. Therefore, those clusters can be easily broken in the particle separator when collided with the separator wall.

In conclusion, we studied the basic principle of the laser ablation ICP-MS for the direct analysis of ceramic powders using the newly designed cyclone-type particle separator. It efficiently removed the heavy particulates and broke the large clusters formed by aggregation. Those mechanisms explained the enhancement of reproducibility and stability in laser ablation ICP-MS measurement. From this study, it also proved that the cell gas and the particle size of powder samples affected on the size of ablated particles and the signals in ICP-MS. In particular the use of the designed separator improved the stability of analytical results for the micron-sized powders in He gas flow. Therefore, although there were still some factors to be optimized, the newly designed cyclone-type separator can successfully be applied for the quantitative analysis of ceramic powders.

Table 1. Physical properties of ceramic powder samples

	ITO	AES-12	MgO	AL-41
Purity (%)	99	99.9	99	99.9
Mean particle size (μm)	0.05	0.5	1	40-60
Tap density (g/cm^3)	2.12	1.76	0.95	1.65

Table 2. Instrumental operating conditions of ICP-MS and laser ablation system

Laser mode	Q-Switched (fixed)
Wavelength	266 nm (fixed)
Energy	3 mJ/pulse
Defocused	10 μm
Repetition rate	10 Hz
Power	1200 W
Nebulizer flow	1.0 L/min
Plasma flow	15 L/min
Auxiliary flow	1.0 L/min
Sweeps/Reading	10
Scan mode	Peak hopping

Experimental

Four ceramic powders with different particle size were prepared. ITO and MgO powders, spotlighted ceramics as a new display material, were prepared by sol-gel method in the size of 50 nm and 1 mm, respectively. The densities of ITO and MgO were measured to be 2.12 and 0.95 g/cm^3, respectively. Two alumina powders, AES12 with high purity and AL-41 with low soda, were purchased from Sumitomo (Japan). The physical properties of the ceramic powders were listed in Table 1.

For laser ablation, the powders were pressed with 1,500 pascal in the diameter of 40 mm using a press (HERZOG PT 40/2D, GmbH Co., Germany). The prepared pellets were ablated and analyzed semi-quantitatively using the laser ablation system (LSX-100, Cetac, Inc., Omaha) equipped with a frequency-quadrupled neodymium-doped yttrium aluminum garnet (Nd:YAG) laser operated under Q-switched mode. The ablated samples were analyzed by ICP-MS (Elan 6000, Perkin-Elmer Sciex, Concord). Typical operating conditions of the laser ablation ICP-MS system were summarized in Table 2. The flow rate of Ar and He gas was adjusted to 1.0 L/min and 0.9 L/min, respectively.

References

1. Becker, J. S. *Spectrochim. Acta Part B* **2002**, *57*, 1805.
2. Zhou, H.; Wang, Z.; Zhu, Y.; Li, Q.; Zou, H.-J.; Qu, H.-Y.; Chen, Y.-R.; Du, Y.-P. *Spectrochim. Acta Part B* **2013**, *90*, 55.
3. Gunther, D.; Hattendorf, B. *Trends in Anal. Chem.* **2005**, *24*, 255.
4. Bleiner, D.; Lienemann, P.; Vonmont, H. *Talanta* **2005**, *65*, 1286.

5. Davide, B.; Peter, L.; Heinz, V. *Talanta* **2005**, *65*, 1286.
6. Guillong, M.; Kuhn, H. R.; Gunther, D. *Spectrochim. Acta Part B* **2003**, *58*, 221.
7. Weis, P.; Beck, H. P.; Gunther, D. *Anal. Bioanal. Chem.* **2005**, *381*, 212.
8. Kuhn, H. R.; Gunther, D. *Anal. Chem.* **2003**, *75*, 747.
9. Koch, J.; Bohlen, A.; Hergenroder, R.; Niemax, K. *J. Anal. At. Spectrom.* **2004**, *19*, 267.
10. Perkins, W. T.; Pearce, N. J. G.; Jeffries, T. E. *Geochim. Cosmochim. Acta* **1993**, *57*, 475.
11. Gonzalez, J.; Mao, X. L.; Roy, J.; Mao, S. S.; Russo, R. E. *J. Anal. At. Spectrom.* **2002**, *17*, 1108.
12. Wang, Z.; Hattendorf, B.; Gunther, D. *J. Anal. At. Spectrom.* **2006**, *21*, 1143.
13. Baker, S. A.; Dellavecchia, M. J.; Smith, B. W.; Winefordner, J. D. *Anal. Chim. Acta* **1997**, *355*, 113.
14. Bleiner, D.; Lienermann, P.; Vonmont, H. *Talanta* **2005**, *65*, 1286.